aerospace

MDPI

Article

Orbital Stability and Invariant Manifolds on Distant Retrograde Orbits around Ganymede and Nearby Higher-Period Orbits

Qingqing Li †, Yuming Tao † and Fanghua Jiang *

School of Aerospace Engineering, Tsinghua University, Beijing 100084, China
* Correspondence: jiangfh@tsinghua.edu.cn
† These authors contribute equally to this work.

Abstract: In the past few years, distant retrograde orbits (DROs) have become increasingly popular due to their conspicuous stability. Nevertheless, it is this characteristic that results in the challenge to the design of transfer orbits into/out of DROs. This paper investigates the DROs around Ganymede in order to utilize their dynamical characteristics for Jupiter system exploration. In particular, the DRO family is calculated by numerical integration and numerical continuation, higher-period orbits near the DROs are detected using bifurcation theory, and characteristics including orbital stability and invariant manifolds of these orbits are investigated through stability indices and manifold theory. The stability of DROs and the higher-period orbits are first investigated in the circular restricted three-body problem and are then verified in a third-body gravitation perturbation model. The results show that the strong stability of DROs makes it possible to observe the Galilean moons for long periods and that the higher-period orbits that bifurcate from the DROs offer additional insight into the motion of probes approaching/departing from the vicinities of the DROs. Further investigation of the invariant manifolds around higher-period orbits reveals the feasibility of utilizing the DRO family and the nearby unstable structures for multi-target exploration and low-energy transfer between the Galilean moons.

Keywords: distant retrograde orbit (DRO); orbital stability; bifurcation; invariant manifold

Citation: Li, Q.; Tao, Y.; Jiang, F. Orbital Stability and Invariant Manifolds on Distant Retrograde Orbits around Ganymede and Nearby Higher-Period Orbits. *Aerospace* **2022**, *9*, 454. https://doi.org/10.3390/aerospace9080454

Academic Editor: Shuang Li

Received: 24 July 2022
Accepted: 16 August 2022
Published: 18 August 2022

1. Introduction

Distant retrograde orbits (DROs) were originally studied by Hénon in his extensive exploration of the whole solution of the planar restricted three-body problem [1]. These orbits are becoming an increasingly popular target for deep space exploration with the Asteroid Redirect Robotic Mission proposed by NASA, which plans to capture an asteroid and then redirect it into a stable orbit, perhaps a DRO around the Moon, as a testbed for potential exploration [2,3]. As deep space exploration increases, several near-time missions have taken the Jupiter system as their target. The Europa Clipper Mission and the Jupiter Icy Moons Explorer (JUICE) mission are expected to be launched no later than 2025 by NASA and ESA, respectively [4,5]. The JAXA's MMX mission will collect observations of Phobos from stable retrograde relative trajectories and aims to reveal the origin of the Martian moons, enhance our comprehension of the Martian system, and pave the way for the human exploration of Mars [6,7]. In order to investigate the application of DROs to Jupiter system exploration, this work will be carried out on the Jupiter–Ganymede system.

The study of the characteristics of DROs began in the 1960s. Hénon first showed that DROs, classified as the family f in his paper, are stable in Hill's problem and have no true upper limit on size [1,8]. At around the same time, Broucke studied periodic orbits, including DROs, called family C in his paper, in the Earth–Moon restricted three-body problem [9]. Based on the f family found by Hénon, Benest explored the stability of retrograde satellites in the circular plane-restricted problem with varying mass ratios

in the mid-1970s [10–12]. At that time, Hénon studied the stability of planar periodic orbits with respect to the perturbations perpendicular to the plane in Hill's limiting case of the restricted three-body problem, and reached the conclusion that the orbits of family f are always stable [13,14]. Since then, several researchers have researched the evolution of DROs in full ephemeris or higher-fidelity dynamical models for different three-body systems [15,16]. This new interest in the study of DROs also motivates researchers to dig further into the possibilities offered by the analytical approach. Lara proposed a perturbation approach to the Hill problem that allows us to provide a very simple low-order analytical solution via trigonometric functions and to compute higher orders of the solution while still depending on special functions [17].

In addition to the characteristics of DROs, the transfer to/from DROs is also a hot research topic. A direct transfer from a low Earth orbit (LEO) to a DRO was studied, both in the circular restricted three-body problem (CR3BP) and in a high-fidelity model of the solar system [18]. For the similar LEO-to-DRO transfer problem, Demeyer et al. examined the possibility of using the hyperbolic network associated with the horizontal Lyapunov orbits around the L_1 point in the Sun–Earth system and found that it can provide transfer orbits to a wider range of DROs with lower budgets of ΔV and/or travel times [19]. Based on the mission of redirecting the captured asteroid to a DRO around the Earth, strategies for DRO transfer design were proposed in the Sun–Earth system [20,21]. In the Jupiter system, some DROs around Europa were explored and a DRO-type capture method was proposed for the transfers to and captures from Europa [22,23]. Recently, McCarthy et al. expanded the DROs to the lunar synodic resonant quasi-DROs, considering natural eclipse avoidance [24].

Due to the interest in long-term space exploration activities, the DRO family, which is linearly stable, offers potential utilizations. However, this stability will pose a challenge to transfer design. In particular, stable and unstable invariant manifolds, typically leveraged for initial guess generation to support transfer design in the CR3BP, are nonexistent. Alternatively, unstable structures that exist in the vicinity of DROs may be available for approaching and departing from those DROs with low energy. To detect the nearby periodic orbit families that may offer useful orbital flows across the region, an in-depth investigation of the dynamical structures in the vicinity of DROs is imperative. The framework for this investigation is based on the identification and exploration of the bifurcations of DROs around Ganymede. We chose Ganymede for our study for two main reasons. First, the mission scenario considered in this paper is one where the probe explores one of the Galilean moons for a set period of time and then transfers to the other Galilean moons to continue the mission. Ganymede lies between Europa and Callisto; thus, the probe can transfer from or to Ganymede, either outward or inward, to achieve multi-target exploration in the Jupiter system. DROs at higher altitudes can be regarded as not being captured by the small body but as being of a higher energy level and with a certain ability of orbital maneuver. Second, the space around Ganymede is less affected by Jupiter's magnetic field and radiation because of its larger distance from Jupiter than Io and Europa, meeting a prerequisite for long-term detection. Meanwhile, Ganymede is the most massive moon in the Jupiter system, and the DRO in the three-body system of Ganymede and Jupiter is less affected by gravitational perturbations from other moons.

The paper is organized as follows. Section 2 introduces the dynamical models and numerical methods that are to be used to compute the periodic orbits and some useful dynamical behavior concerning stability, bifurcations, and invariant manifolds. In Section 3, the Ganymede DRO family and bifurcating periodic orbits in the CR3BP and their linear stability are first presented. The results of exploring bifurcations motivate a further investigation to exploit the invariant manifold structures for a transfer design. In addition, a perturbation model is employed to verify the feasibility and accuracy of solutions in the CR3BP. In the last section, our conclusions are presented.

2. Dynamical Model, Numerical Methods, and Dynamical Theories

This section introduces the dynamical model used in this work, the numerical methods employed to compute the families of periodic solutions in the CR3BP, and the dynamical theories applied to investigate the bifurcation of orbits, the linear stability of periodic orbits, and invariant manifold structures around unstable orbits.

2.1. The Circular Restricted Three-Body Problem

Ganymede has an orbital eccentricity of 0.0013, which is very small; this means that the CR3BP can be used to provide an approximation of Jupiter–Ganymede dynamics. The dynamical model in the CR3BP consists of three bodies, with masses m_1, m_2, and m_3. The third body m_3 is massless compared to the two primaries, m_1 and m_2, without the loss of generality, assuming $m_1 > m_2$. The CR3BP assumes that two primary bodies are moving in a circular orbit about their common barycenter and that the motion of m_3 is dominated by the gravitational attractions of them. Conventionally, the system is normalized, such that both the distance between m_1 and m_2, LU, and the mean motion of the primaries, WU, are constant and equal to unity, which means that the orbital period of m_2 is 2π time units. In addition, let μ denote the ratio of the mass of the secondary body to the total mass, so that the first and secondary primaries' masses are nondimensional and equal to $1-\mu$ and μ, respectively. The motion of the third body is then described using a normalized dimensionless synodic system. The synodic system is a rotating coordinate system, with its origin at the barycenter of the primaries, an x-axis directed from the origin in a direction away from the primary, a y-axis aligned with the direction of the velocity vector of the secondary, and a z-axis completing the right-handed coordinate system, as depicted in Figure 1. In this rotating frame, the equations of motion for the third body are written thus, as seen in [25]:

$$\begin{cases} \ddot{x} - 2\dot{y} = \frac{\partial U}{\partial x} \\ \ddot{y} + 2\dot{x} = \frac{\partial U}{\partial y} \\ \ddot{z} = \frac{\partial U}{\partial z} \end{cases} \tag{1}$$

where U denotes the pseudo-potential expressed thus, as seen in [25]:

$$U = \frac{x^2 + y^2}{2} + \frac{1-\mu}{r_1} + \frac{\mu}{r_2} \tag{2}$$

with r_1 and r_2 defined thus, as seen in [25]:

$$r_1 = \sqrt{(x+\mu)^2 + y^2 + z^2} \qquad r_2 = \sqrt{(x-1+\mu)^2 + y^2 + z^2}. \tag{3}$$

Equation (1) admits an energy-like integral of the motion, called the Jacobi constant, which serves to characterize the families of trajectories and is written thus, as seen in [25]:

$$J = x^2 + y^2 + \frac{2(1-\mu)}{r_1} + \frac{2\mu}{r_2} + \mu(1-\mu) - \left(v_x^2 + v_y^2 + v_z^2\right). \tag{4}$$

To describe the simplified Jupiter–Ganymede system, $\mu = 7.8063 \times 10^{-5}$, $LU = 1.0704 \times 10^6$ km and $WU = 1.0164 \times 10^{-5}$ rad/s are used in this work.

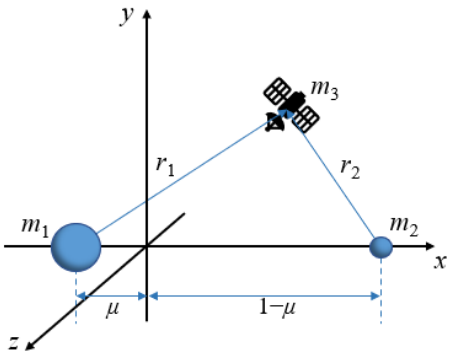

Figure 1. Dimensionless synodic frame.

2.2. Numerical Methods

Solutions that are symmetric about the x-axis and the x–z plane are evident from the symmetry in Equation (1). For the application of the periodicity theorem proposed by Roy and Ovenden [26] for the CR3BP, it is immediately obvious that a trajectory that perpendicularly crosses the x–z plane or the x-axis twice is a closed periodic orbit. Therefore, there are actually three possible types of symmetric periodic solutions in the CR3BP: an axis-symmetric (AS) orbit, which has two perpendicular crossings of the x-axis, a plane-symmetric (PS) orbit, which has two perpendicular crossings of the x–z plane, and a doubly symmetric (DS) orbit, which satisfies an AS configuration and a PS configuration [27–29]. In this work, DROs, which belong to the AS orbits in the planar CR3BP, are investigated.

Let $[x_0, 0, 0, 0, v_{y0}, 0]^T$ denote the initial state of a DRO, where $y_0 = 0$, $z_0 = 0$, $v_{x0} = 0$, and $v_{z0} = 0$ indicate that the planar orbit perpendicularly crosses the plane $y = 0$ at the initial time. To obtain a periodic, symmetric, and planar orbit, this initial state will be propagated forward in time for half a period, when this orbit should perpendicularly cross the plane $y = 0$ once again. In this work, the MATLAB function, ODE45, is employed to solve the dynamical differential equations of DR3BP. Specifically, we set both the absolute and relative error tolerance of 10^{-10} and use the "Events" option to specify that the integration terminates at a zero where the event function is increasing. The steps of numerical computation that are used to achieve a family of symmetric periodic orbits are summarized as follows. First, given the initial position x_0, the initial velocity v_{y0} can be calculated in the two-body system; thus, we have the initial guess for a starting point. Next, dichotomy or differential correction can be used to correct v_{y0}, such that the orbit will pass perpendicularly through the plane $y = 0$; thus, the first orbit is found. Then, by means of numerical continuation with respect to x_0, a family of orbits can be obtained.

2.2.1. Dichotomy

Since only one variable needs to be adjusted, we can use dichotomy to establish a sufficiently precise initial value. Generally, we choose 0.1 or 0.01 as the length of the dichotomy interval for the dimensionless variable v_{y0} after normalization. Unless otherwise stated, the following calculations and drawings are carried out in the normalized coordinate system. Qualitatively, when the probe passes through the plane $y = 0$, the centripetal or centrifugal trend of the probe can be determined by judging the direction of the velocity vector (or the direction of v_x), as shown in Figure 2, where the middle orbital is perpendicular to the x-axis, the left orbital has $v_x < 0$, and the right orbital has $v_x > 0$. Then, the initial velocity value is corrected by dichotomy. This method has a high convergence speed for calculating two-dimensional periodic orbits with good symmetry, but its disadvantages are that the convergence range is small, the input guess initial value cannot differ too much from the "exact value", and the length of the dichotomy interval cannot be too large. When the problem is extended to three dimensions, the dichotomy method fails. At that time, a shooting correction method for the state transition matrix is still needed.

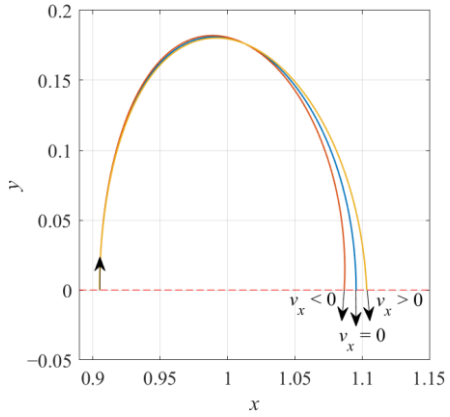

Figure 2. Judgment condition of dichotomy.

2.2.2. Differential Correction

The state transition matrix (STM), the product of which, with the state vector at an initial time t_0, gives the state vector at a later time t, is denoted by $\boldsymbol{\Phi}(t, t_0)$ here. Considering the three-dimensional orbits that are symmetric about the plane $y = 0$, let $[x_0, 0, z_0, 0, v_{y0}, 0]^{\mathrm{T}}$ denote the initial state of the orbit. If correction is not performed, the state when the probe passes through the plane $y = 0$ can be expressed as $[x, 0, z, v_x, v_y, v_z]^{\mathrm{T}}$. When fix z_0 and correct x_0 and v_{y0}, the first-order relationship between the free variables and the boundary values at half a period can be expressed thus, as seen in [30]:

$$\begin{bmatrix} \delta v_{x,T/2} \\ \delta v_{z,T/2} \end{bmatrix} = \begin{bmatrix} \varphi_{41} - \frac{\dot{v}_x \varphi_{21}}{\dot{y}} & \varphi_{45} - \frac{\dot{v}_x \varphi_{25}}{\dot{y}} \\ \varphi_{61} - \frac{\dot{v}_z \varphi_{21}}{\dot{y}} & \varphi_{65} - \frac{\dot{v}_z \varphi_{25}}{\dot{y}} \end{bmatrix} \begin{bmatrix} \delta x_0 \\ \delta v_{y0} \end{bmatrix} \tag{5}$$

where φ_{ij} denotes the element in the ith row and the jth column of $\boldsymbol{\Phi}(T/2, t_0)$. Based on this relationship, the initial condition of a periodic orbit is calculated when $v_{x,T/2}$ and $v_{z,T/2}$ are reduced to a defined small value by several iterations. If the problem is a two-dimensional one, Equation (5) can be simplified as:

$$\delta v_{x,T/2} = \left(\varphi_{45} - \frac{\dot{v}_x \varphi_{25}}{\dot{y}} \right) \delta v_{y0}. \tag{6}$$

2.3. Orbital Stability

The monodromy matrix is the STM evaluated after one period along a periodic solution, written as $\boldsymbol{M} = \boldsymbol{\Phi}(t_0 + T, t_0)$. For more details of the monodromy matrix, readers are referred to Ref. [31]. In the CR3BP, the second-order system possesses three degrees of freedom and, thus, $\boldsymbol{M}$ is defined in terms of six eigenvalues. First, because the monodromy matrix is a symplectic map, if λ_i is an eigenvalue of the matrix $\boldsymbol{M}$, then $1/\lambda_i$ is also an eigenvalue. Second, because the monodromy matrix is associated with a periodic solution, at least one unity eigenvalue will always exist. Furthermore, the fact that eigenvalues of matrix $\boldsymbol{M}$ must come in reciprocal pairs results in at least two unity eigenvalues. Thus, the set of eigenvalues from the monodromy matrix for a particular periodic orbit occurs in the form $(\lambda_1, 1/\lambda_1, \lambda_2, 1/\lambda_2, \lambda_3, 1/\lambda_3)$, where λ_i represents the eigenvalue of $\boldsymbol{M}$ and $\lambda_1 = 1/\lambda_1 = 1$. The eigenvalues of matrix $\boldsymbol{M}$ are used to assess the stability characteristics of a periodic orbit in a linear sense. The eigenvalue with a magnitude greater than one indicates instability, while the eigenvalue with a magnitude equal to one reflects orbit periodicity, and the eigenvalue with a magnitude less than one indicates stability. Accordingly, the linear stability of an orbit can be described by stability indices, which are defined thus, as seen in [9,32,33]:

$$\nu_i = \frac{1}{2}\left(\|\lambda_i\| + \frac{1}{\|\lambda_i\|} \right), \; i = 1, 2, 3. \tag{7}$$

If all the stability indices are equal to unity, the orbit is said to be linearly stable and possesses neither stable nor unstable manifolds; if any stability index is greater than unity, the orbit is considered unstable, and invariant manifolds that approach and depart from the periodic orbit will exist. Evidently, the stability index that corresponds to the two unity eigenvalues is always equal to unity. Therefore, merely considering the other two indices, in the case where they are both equal to unity, the linear instability of the orbit is order zero; in cases where they are both greater than unity, the linear instability of the orbit is order two; otherwise, the linear instability of the orbit is order one. That is to say, the linear instability in this system can be of orders zero, one, or two. The order of orbital instability yields the linear stability level of the orbits. A periodic orbit with instability order zero is the most stable orbit, in a linear sense.

2.4. Bifurcations

In dynamical systems, a change in the stability of the periodic orbits results in a bifurcation. There are three distinct ways in which the stability can change, denoted by a tangent bifurcation, period-doubling bifurcation, and secondary Hopf bifurcation, respectively. In addition, other types of bifurcation occur along the original solution without a change in the order of instability, such as period-multiplying bifurcations and a modified secondary Hopf bifurcation. For more details on bifurcations, readers are referred to Ref. [34]. The stability of a periodic orbit reflects the behavior of nearby trajectories; thus, monitoring the eigenvalues of the monodromy matrix corresponding to each periodic orbit in a family is a good method by which to detect and characterize the local bifurcations.

In 1969, Broucke [35] introduced an alternative method to discuss stability, based on two stability coefficients of the orbit, α and β:

$$\begin{aligned} \alpha &= -\left(\lambda_2 + \tfrac{1}{\lambda_2} + \lambda_3 + \tfrac{1}{\lambda_3}\right) = 2 - \mathrm{Tr}(\boldsymbol{M}) \\ \beta &= \tfrac{1}{2}\left[\alpha^2 - \left(\lambda_2{}^2 + \tfrac{1}{\lambda_2{}^2} + \lambda_3{}^2 + \tfrac{1}{\lambda_3{}^2}\right)\right] = \tfrac{1}{2}\left[\alpha^2 + 2 - \mathrm{Tr}(\boldsymbol{M}^2)\right] \end{aligned} \tag{8}$$

In this technique, four nontrivial eigenvalues of the monodromy matrix for each family member are fully defined by the scalars α and β. The Broucke stability diagram in Figure 3a offers insight into the orbital stability in the α-β plane. A more informative stability diagram [34], based on the Broucke stability diagram, is constructed as shown in Figure 3b. Each periodic orbit may be represented by a point in Figure 3b; thus, a curve that illustrates a family of periodic orbits can be drawn. Bifurcations occur when this curve intersects those in Figure 3b and bifurcation points, namely, intersections are found. In Table 1, bifurcation types are described with the equations of curves in Figure 3b.

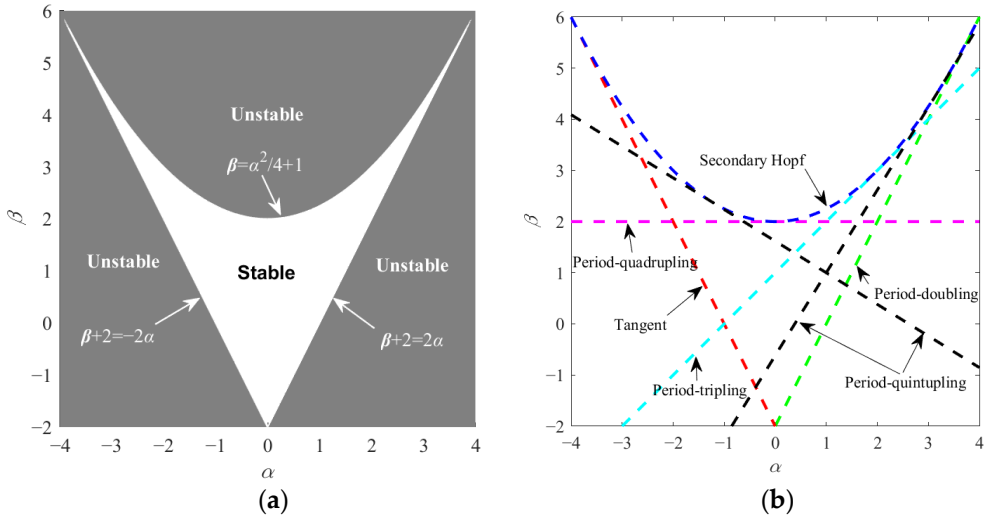

Figure 3. (**a**) Broucke stability diagram and (**b**) stability diagram.

Table 1. Classification of bifurcations, based on the stability diagram.

Bifurcation Type	Equation of Curve Representing Bifurcation
Tangent	$\beta + 2 = -2\alpha$
Period-doubling	$\beta + 2 = 2\alpha$
Period-tripling	$\beta = \alpha + 1$
Period-quadrupling	$\beta = 2$
Period-quintupling	$\beta = 1/(2\cos(4\pi/5))\ \alpha - (\cos(8\pi/5) + 1)/\cos(4\pi/5)$ $\beta = 1/(2\cos(8\pi/5))\ \alpha - (\cos(16\pi/5) + 1)/\cos(8\pi/5)$
Secondary Hopf	$\beta = \alpha^2/4 + 1, -4 < \alpha < 4$

2.5. Invariant Manifolds

Invariant stable and unstable manifolds are considered in this work. If the probe moves on the stable manifolds of a periodic orbit, it will asymptotically approach that orbit without providing external energy; if it moves on unstable manifolds, it will asymptotically depart from that orbit without providing external energy. Accordingly, invariant manifolds can be leveraged to design low-energy orbital transfer. Consider a periodic orbit that possesses one pair of stable and unstable eigenvalues, indicated by $|\lambda_s| < 1$ and $|\lambda_u| > 1$. Correspondingly, there is a pair of stable and unstable eigenvectors, indicated by $\boldsymbol{e}_s$ and $\boldsymbol{e}_u$. The invariant manifolds corresponding to the propagations of $\boldsymbol{e}_s$ and $-\boldsymbol{e}_s$ are stable manifolds, while those corresponding to the propagations of $\boldsymbol{e}_u$ and $-\boldsymbol{e}_u$ are unstable manifolds. For a point of an unstable orbit, $\boldsymbol{x}_o$, we introduce a small disturbance in the direction of the corresponding eigenvectors, thereby producing initial conditions for the stable and unstable manifolds, $\boldsymbol{x}_{s,0}$ and $\boldsymbol{x}_{u,0}$, respectively:

$$\boldsymbol{x}_{s,0} = \boldsymbol{x}_o \pm \varepsilon \boldsymbol{e}_s \quad \boldsymbol{x}_{u,0} = \boldsymbol{x}_o \pm \varepsilon \boldsymbol{e}_u \tag{9}$$

where ε is a sufficiently small real-valued number. The stable and unstable manifolds at this point can be computed by propagating the initial conditions forward and backward in time, respectively. Note that when dissipative forces are considered, the manifold obtained above needs to be modified in the initial value, or halfway, to achieve the transfer orbit between the target bodies. If we discretize the orbit into numerous points and repeat the steps above, then the stable and unstable manifold structures are obtained [36,37]. For orbits that have complex geometric configurations, such as period-multiplying orbits, drawing manifolds directly is detrimental to subsequent analysis; therefore, a Poincaré section is employed to delineate the manifold structures in this case.

3. The Ganymede DRO Family and Its Bifurcations

3.1. The DRO Family and Its Linear Stability

A resonant DRO (2:1) and its direction of motion in the synodic frame and in the Jupiter-centered inertial frame are shown in red in subgraphs (a) and (b) of Figure 4, respectively. It is evident that the DRO around the secondary body is in a direction opposite to the direction of the secondary body orbiting around the barycenter when viewed in the rotating frame, and orbits in a prograde direction following the secondary body when viewed in the inertial frame; hence, it is called a distant retrograde orbit (DRO).

Considering the positions and perturbations of the other three Galilean moons, the DRO family whose initial position x_0 covers from 0.9 to 0.995 with an interval of 0.0005 is calculated, as shown in Figure 5. Each color of orbit indicates each Jacobi constant value, as specified by the color bar on the right. Jupiter and the four Galilean moons' orbits around Jupiter are drawn to real proportion. It is apparent that the DROs orbiting closer to Ganymede possess higher Jacobin constant values, which can be as high as the Jacobin constant values for L_1 and L_2. Figure 6 shows that the three stability indices of DROs are equal to unity; namely, all the orbits of this family are linearly stable.

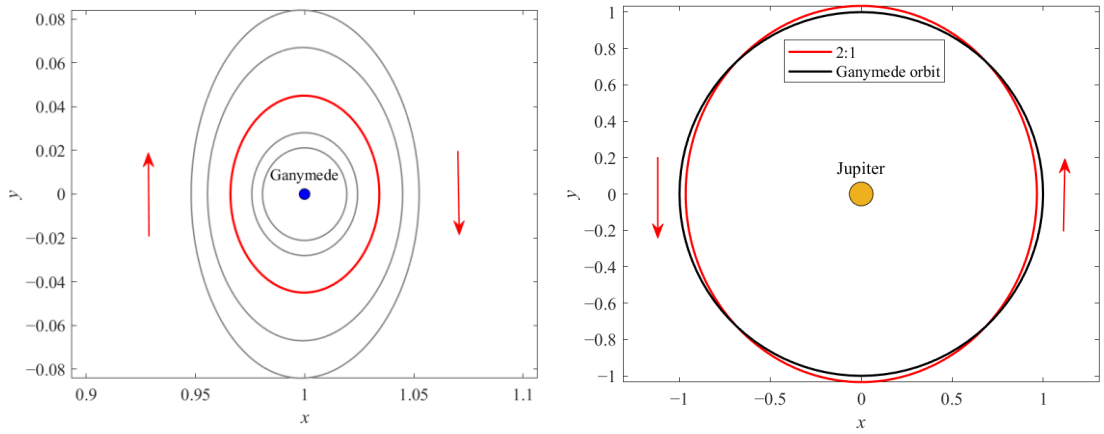

Figure 4. (**a**) Several DROs in the synodic frame (2:1 resonant DRO: $\boldsymbol{X}_0 = [0.9660, 0, 0, 0, 0.094231, 0]^{\mathrm{T}}$) and (**b**) 2:1 resonant DRO in the inertial frame with Ganymede orbit.

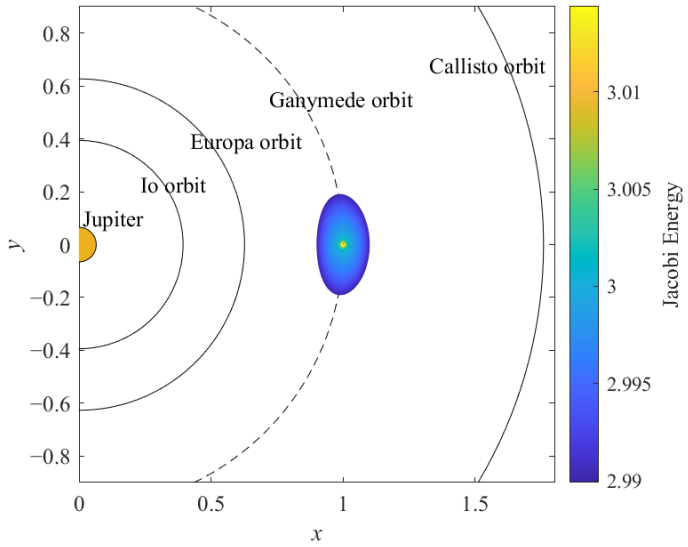

Figure 5. The DRO family in the Jupiter–Ganymede rotating frame, in real proportion.

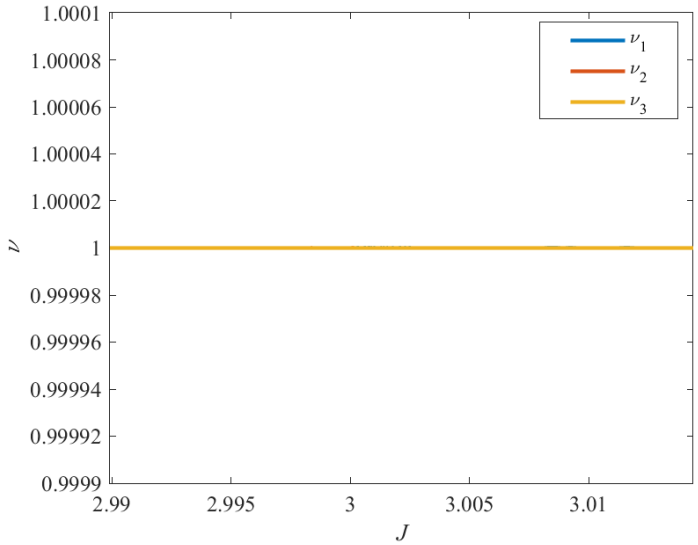

Figure 6. Stability indices of DROs.

3.2. Bifurcations of DROs

As indicated by the stability indices, DROs cannot be targeted with a low-energy transfer along stable and unstable manifolds, as with unstable orbits in the CR3BP. Therefore, alternative strategies are necessary to understand and exploit the natural flows in the vicinity of the DROs. In dynamical systems, a bifurcation may result in a new family of periodic orbits intersecting with the current family, and it is in this new family that useful stable and unstable manifold structures may arise. Bifurcation theory is applied to give a further investigation of the dynamical structures in the DRO vicinity, providing insight into the complex trajectory behavior in this region.

3.2.1. DRO Stability Diagram

In Figure 7, a colorful curve is plotted on the stability diagram that corresponds to the DRO family. The color of each point indicates the Jacobi constant value for this orbit. In this figure, colored asterisks reflect the bifurcation points that correspond to bifurcations with the same color. Evidently, period-tripling, period-quadrupling, and period-quintupling bifurcations occur. To easily recognize these bifurcating orbits and the corresponding families to which they belong, a naming convention [33] for these new families is necessary. For period-multiplying bifurcations, the naming format is defined as follows: "PmDRO$_n$", where "Pm" refers to the order of the period-multiplication (e.g., period-tripling is reflected as m = 3), and "n" denotes a sub-family identifier (i.e., for multiple bifurcations of the same type, the first family, in order of increasing initial position x_0, is labeled n = 1, the second family is labeled n = 2, etc.). Accordingly, new families originating from period-tripling bifurcation are named P3DRO$_1$, P3DRO$_2$, and P3DRO$_3$; new families originating from period-quadrupling bifurcation are named P4DRO$_1$ and P4DRO$_2$; new planar families originating from period-quintupling bifurcation are named P5DRO$_1$ and P5DRO$_2$. Employing the numerical methods stated in the previous section, all the new families of periodic orbits originating at each of these bifurcations are computed. In Sections 3.2.2–3.2.4, the bifurcating orbits and their stability are investigated to find the underlying unstable manifold structures for low-energy transfer design between DROs.

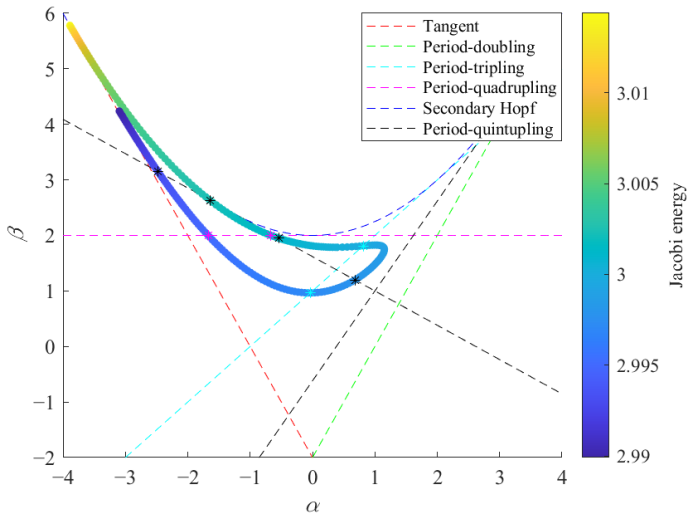

Figure 7. DRO stability diagram.

3.2.2. Period-Tripling Bifurcation

The P3DRO families and their linear stability are studied in this subsection. The characteristics of orbits in the P3DRO$_1$, P3DRO$_2$, and P3DRO$_3$ families are illustrated in Figures 8a, 9a and 10a, respectively. In Figures 8b, 9b and 10b, a member from each of these new families is computed and plotted in the synodic system to illustrate their complex multi-revolution geometries, along with their unique and distinct characteristics. In each of

these figures, an orbit of new periodic families is plotted in green, along with a DRO of the same initial position x_0 in black, while Ganymede appears as a blue sphere, and the initial point along each trajectory is marked with an asterisk.

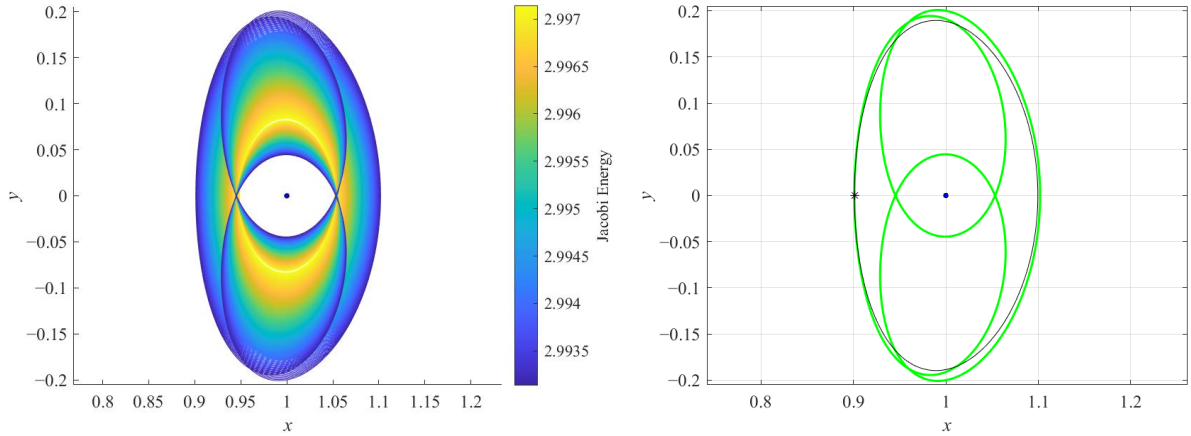

Figure 8. Orbits plotted in the Jupiter–Ganymede rotating frame: (**a**) P3DRO$_1$ family and (**b**) P3DRO$_1$ ($\boldsymbol{X}_0$ = [0.9010, 0, 0, 0, 0.19928, 0]$^{\mathrm{T}}$) and DRO ($\boldsymbol{X}_0$ = [0.9010, 0, 0, 0, 0.20722, 0]$^{\mathrm{T}}$) at x_0 = 0.9010.

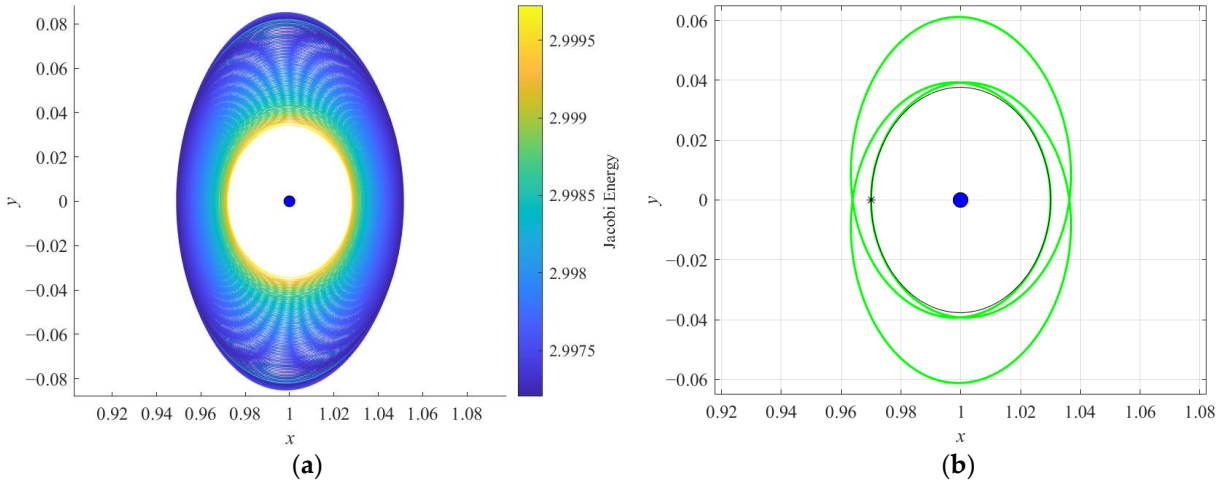

Figure 9. Orbits plotted in the Jupiter–Ganymede rotating frame: (**a**) P3DRO$_2$ family and (**b**) P3DRO$_2$ ($\boldsymbol{X}_0$ = [0.9700, 0, 0, 0, 0.09365, 0]$^{\mathrm{T}}$) and DRO ($\boldsymbol{X}_0$ = [0.9700, 0, 0, 0, 0.09062, 0]$^{\mathrm{T}}$) at x_0 = 0.9700.

The families of period-tripling bifurcating orbits possess periods that are approximately three times the period of the DROs, and the periods decrease as the orbits approach Ganymede. Each family possesses different levels of Jacobi energy and different geometries. The P3DRO$_1$ family possesses a Jacobi energy of less than 2.9972. Orbits in this family are a long distance from Ganymede, even though they propagate from a position far from Ganymede to a closer one. The P3DRO$_2$ family with a Jacobi energy from 2.9972 to 2.9998 closely approximates a DRO-like motion, albeit periodic, with three Ganymede passes instead of one. The P3DRO$_3$ family possesses a Jacobi energy greater than 2.9998. Some of the larger members of this family offer positions close enough to Ganymede; note that, with a further extension of this family, the members with higher Jacobi energy will pass inside Ganymede's radius. This property may prove useful in landing or impact missions. Figure 11 presents the stability information of period-tripling bifurcating orbits. Apparently, only the orbits at the bifurcation points are linearly stable, while the other orbits are linearly unstable, with a maximum index from 1 to 35. Accordingly, the unstable P3DRO families

can be taken into consideration when designing low-energy trajectories in the vicinity of the DROs.

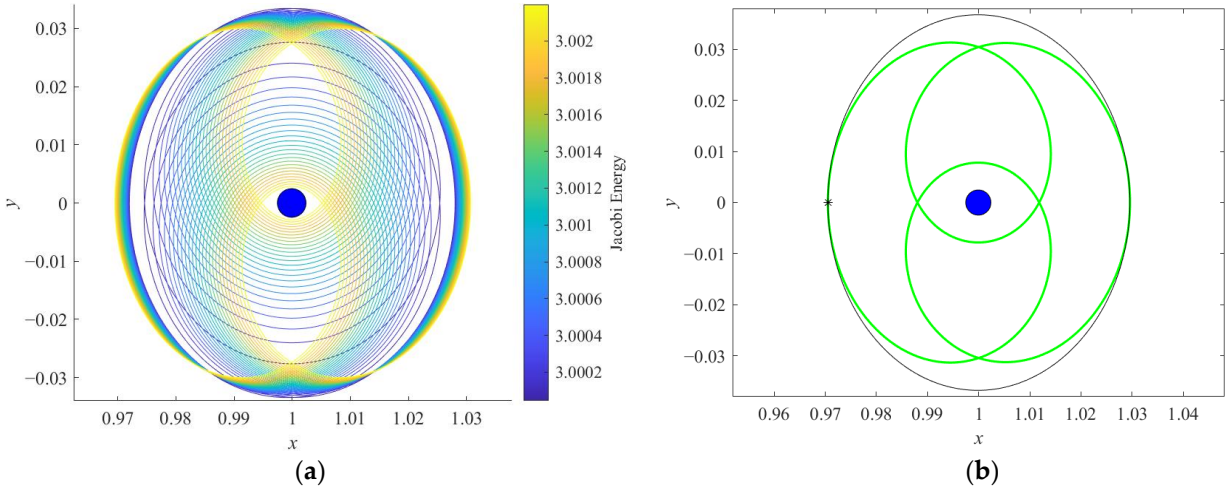

(**a**) (**b**)

Figure 10. Orbits plotted in the Jupiter–Ganymede rotating frame: (**a**) P3DRO$_3$ family and (**b**) P3DRO$_3$ ($\boldsymbol{X}_0$ = [0.9705, 0, 0, 0, 0.07974, 0]$^{\mathrm{T}}$) and DRO ($\boldsymbol{X}_0$ = [0.9705, 0, 0, 0, 0.09023, 0]$^{\mathrm{T}}$) at x_0 = 0.9705.

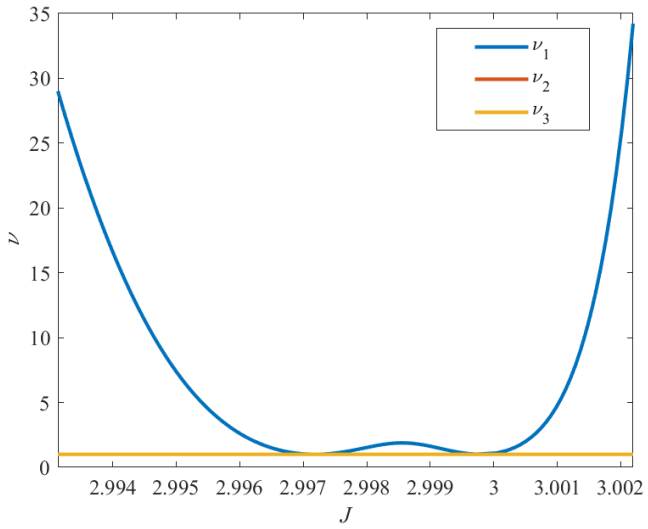

Figure 11. Stability indices of P3DRO families.

3.2.3. Period-Quadrupling Bifurcation

The P4DRO families and their linear stability are studied in this subsection. The P4DRO$_1$ and P4DRO$_2$ families appear in Figures 12 and 13, following the same convention as the period-tripling bifurcation, respectively. Orbits in the P4DRO$_1$ family possess a Jacobi energy of less than 2.9951, while orbits in the P4DRO$_2$ family possess a Jacobi energy larger than 3.0013. In contrast to the P4DRO$_1$ family, the P4DRO$_2$ family has a smaller size and exists in the vicinity of Ganymede. A range of orbits in the P4DRO$_2$ family can reach within the radius of Ganymede (not pictured here), while the portion plotted here offers a fully low altitude. These new families of periodic orbits that are calculated here are linearly stable or nearly stable, as delineated in Figure 14, which means that there is no manifold structure available by which to design low-energy transfer orbits.

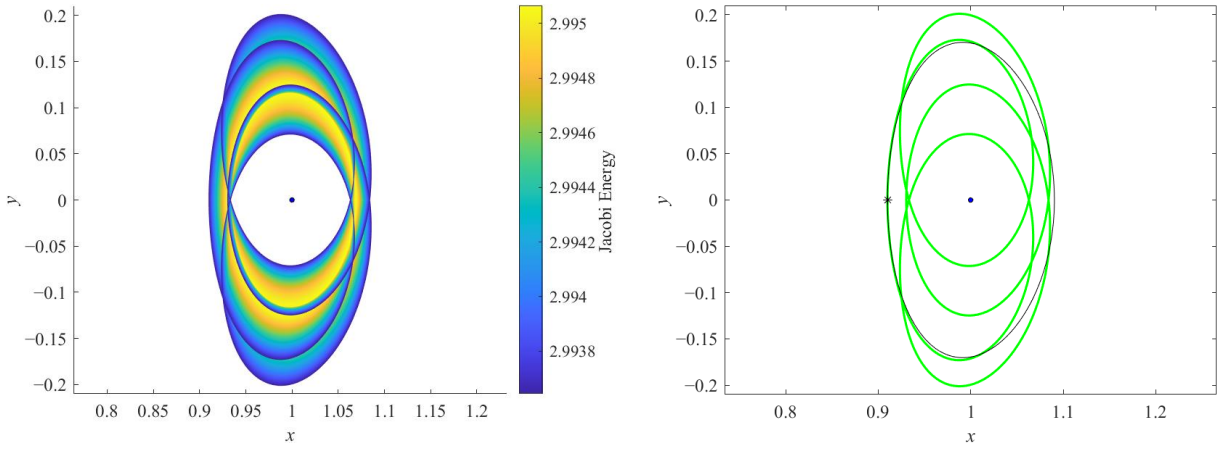

Figure 12. Orbits plotted in the Jupiter–Ganymede rotating frame: (**a**) P4DRO$_1$ family and (**b**) P4DRO$_1$ ($\boldsymbol{X}_0$ = [0.9100, 0, 0, 0, 0.18361, 0]$^{\mathrm{T}}$) and DRO ($\boldsymbol{X}_0$ = [0.9100, 0, 0, 0, 0.18905, 0]$^{\mathrm{T}}$) at x_0 = 0.9100.

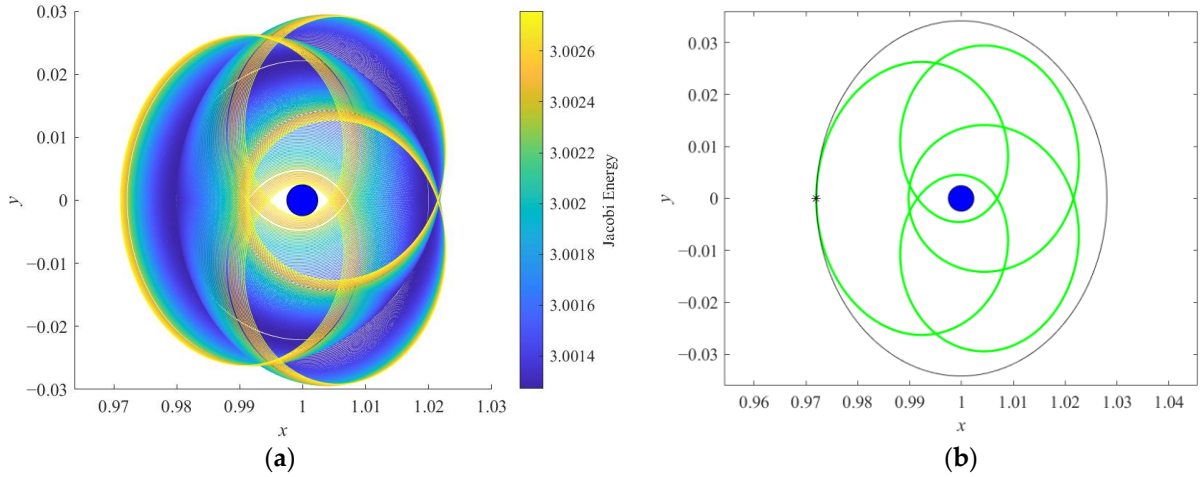

Figure 13. Orbits plotted in the Jupiter–Ganymede rotating frame: (**a**) P4DRO$_2$ family and (**b**) P4DRO$_2$ ($\boldsymbol{X}_0$ = [0.9720, 0, 0, 0, 0.07323, 0]$^{\mathrm{T}}$) and DRO ($\boldsymbol{X}_0$ = [0.9720, 0, 0, 0, 0.08917, 0]$^{\mathrm{T}}$) at x_0 = 0.9720.

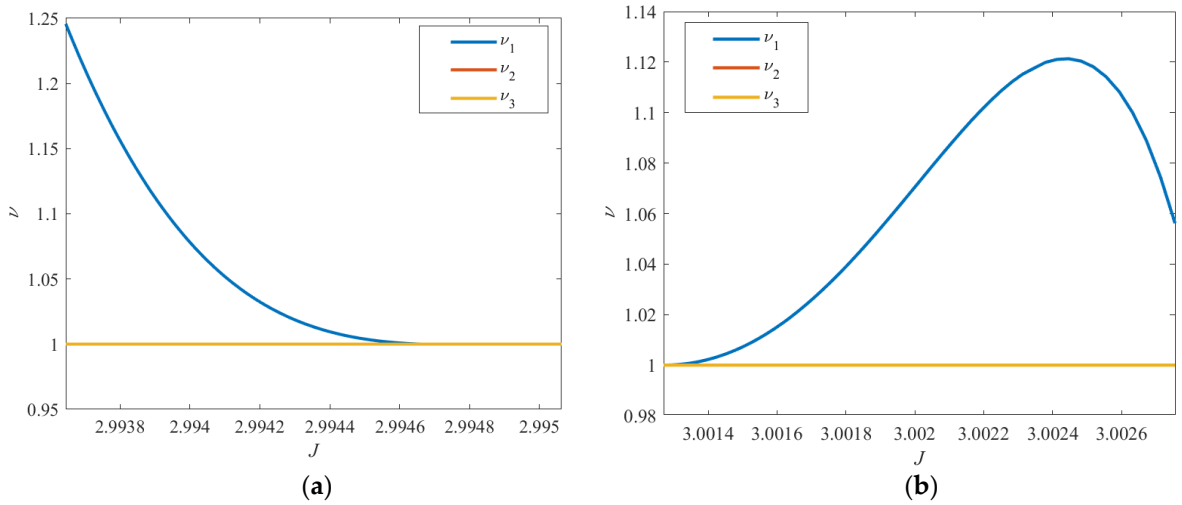

Figure 14. Stability indices of P4DRO families: (**a**) P4DRO$_1$ family and (**b**) P4DRO$_2$ family.

3.2.4. Period-Quintupling Bifurcation

The P5DRO families and their linear stability are studied in this subsection. According to the stability diagram for DROs, two planar families and two three-dimensional families of period-quintupling bifurcating orbits are identified. In this investigation, only two planar families of period-quintupling bifurcating orbits, namely, $P5DRO_1$ with a Jacobi energy of less than 2.9931 and $P5DRO_2$, with a Jacobi energy larger than 3.0023, are discussed. Note that, for the $P5DRO_2$ family, two trajectories of different multi-revolution geometries may exist while sharing the same Jacobi energy. Figures 15–17 illustrate the family $P5DRO_1$ and two sub-$P5DRO_2$ families with different structures, respectively. The $P5DRO_1$ family is far from Ganymede, has a larger size, and possesses a low level of Jacobi energy, while the $P5DRO_2$ family has a smaller size, where the orbit sometimes moves very close to Ganymede. A remarkable distinction between the two sub-$P5DRO_2$ is that in the synodic system, the third body orbits Ganymede inward and outward, as shown in Figures 16 and 17, respectively. As indicated in Figure 18, the planar families of period-quintupling bifurcating orbits are linearly stable or nearly stable.

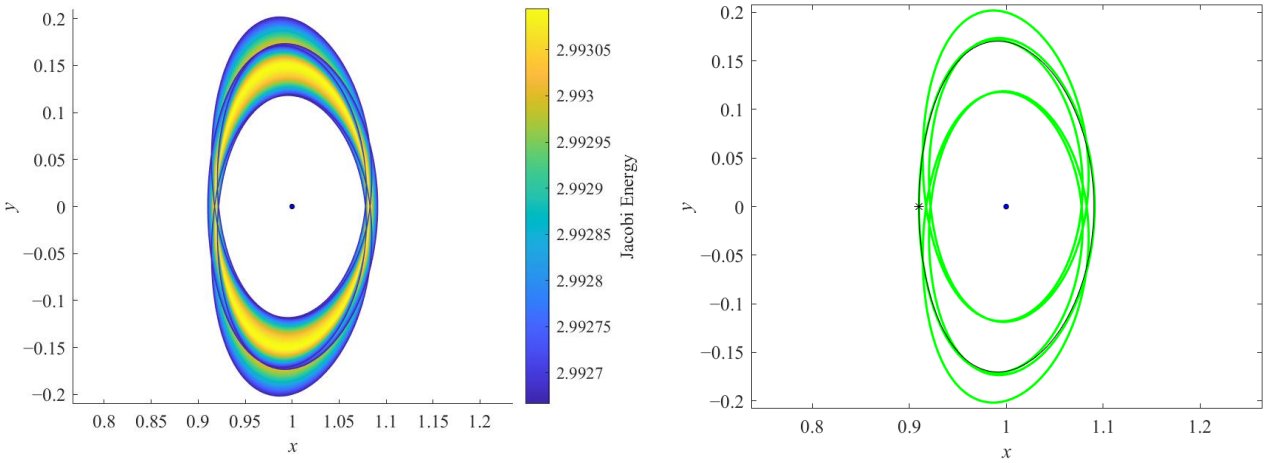

Figure 15. Orbits plotted in the Jupiter–Ganymede rotating frame: (**a**) $P5DRO_1$ family and (**b**) $P5DRO_1$ (X_0 = [0.9100, 0, 0, 0, 0.18625, 0]^T) and DRO (X_0 = [0.9100, 0, 0, 0, 0.18905, 0]^T) at x_0 = 0.9100.

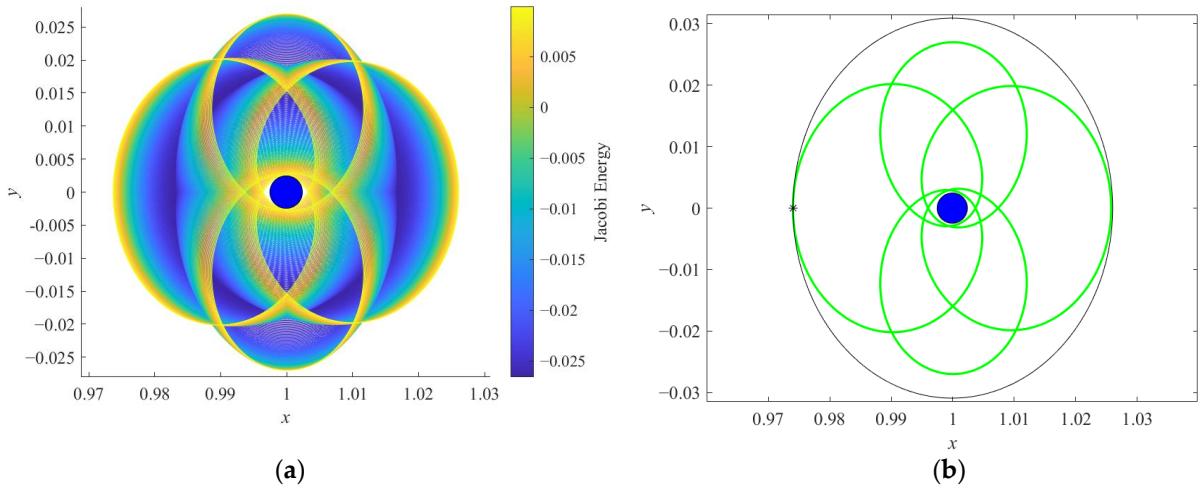

Figure 16. Orbits plotted in the Jupiter–Ganymede rotating frame: (**a**) one sub-$P5DRO_2$ family and (**b**) $P5DRO_2$ (X_0 = [0.9740, 0, 0, 0, 0.06440, 0]^T) and DRO (X_0 = [0.9740, 0, 0, 0, 0.08800, 0]^T) at x_0 = 0.9740.

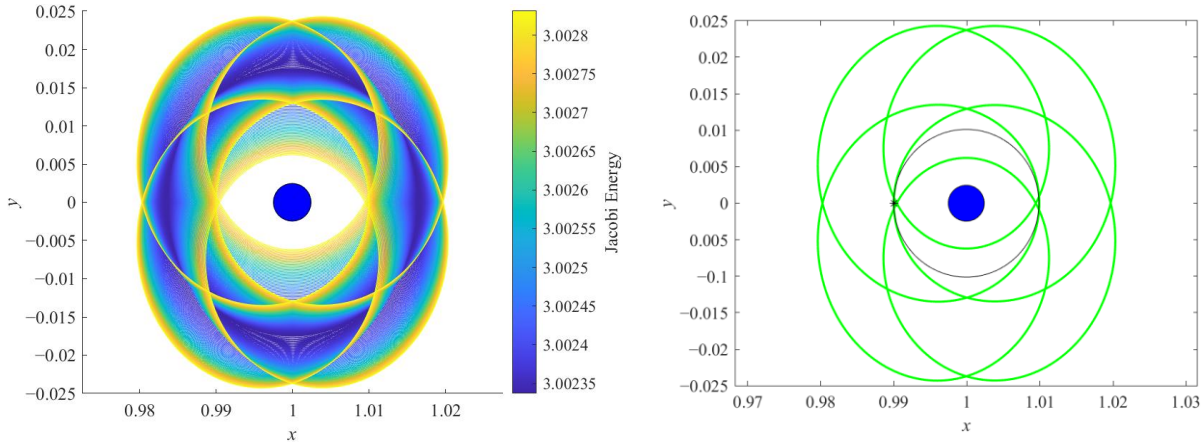

Figure 17. Orbits plotted in the Jupiter–Ganymede rotating frame: (**a**) the other sub-P5DRO$_2$ family and (**b**) P5DRO$_2$ ($\boldsymbol{X}_0$ = [0.9900, 0, 0, 0, 0.11387, 0]$^{\mathrm{T}}$) and DRO ($\boldsymbol{X}_0$ = [0.9900, 0, 0, 0, 0.09956, 0]$^{\mathrm{T}}$) at x_0 = 0.9900.

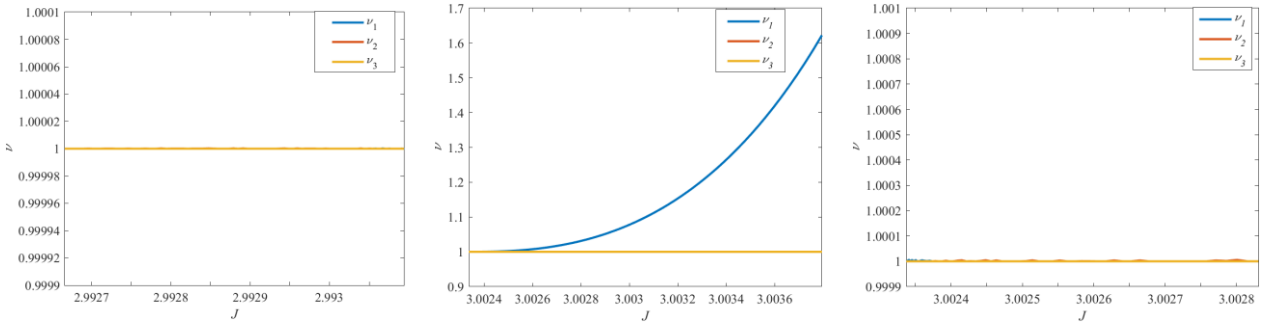

Figure 18. Stability indices of P4DRO families: (**a**) P5DRO$_1$ family, (**b**) one sub-P5DRO$_2$ family shown in Figure 16a, and (**c**) the other sub-P5DRO$_2$ family shown in Figure 17a.

3.3. Analysis of Perturbations

Previous research [38] focuses on the perturbations of the low orbit of Europa (100~400 km of altitude). At this altitude, Europa's gravitational influence is dominant, while the gravitational influence of other moons is not obvious. The DROs around Ganymede that we are studying are at higher altitudes of more than 3000 km, even reaching 100,000 km. The DROs are also dominated by the gravitational influence of Jupiter and Ganymede. The higher orbits would increase the gravitational influence of Europa or Callisto, especially for the unstable bifurcation orbits of DROs, while the gravitational perturbations of other moons will disrupt the structure of the bifurcation orbits.

In the Jupiter–Ganymede CR3BP system without any perturbation, the DROs around Ganymede are stable. However, because of the special periodic resonance relationship between the Galilean moons and their short period characteristics, the perturbations cannot be ignored for practical missions. Thus, the gravitations of the Galilean moons and the Sun are considered as perturbations in this work, to investigate the time evolution of a massless body orbiting Jupiter. Here, we use an inertial frame with Jupiter at its center, while the Galilean moons and the Sun are moving in circular orbits about the origin of this coordinate system.

The initial condition $\boldsymbol{X}_0$ of a DRO can be calculated in the CR3BP system, then transformed to the inertial system and given the Galilean moons' and the Sun's initial phase angles θ_{i0} (i = 1, 2, 3, 4) and θ_{s0}, respectively. The DRO affected by their gravitational perturbations can be obtained by propagating $\boldsymbol{X}_0$ forward. One example of perturbed

DRO at $\boldsymbol{X}_0 = [0.9400, 0, 0, 0, 0.13208, 0]^{\mathrm{T}}$ with $\theta_{i0} = 0$ and $\theta_{s0} = 0$ and a propagation time of 1 year is shown in Figure 19. The influence of the Sun's gravity in the Jupiter system is very small, so the main perturbation influence comes from the other Galilean moons. Meanwhile, the investigated DRO is a considerable distance from the other Galilean moons, as shown in Figure 19b. Therefore, the perturbed DRO remains in a similar trajectory to the DRO, without any perturbation within the given propagation time. When this trajectory crosses the $y = 0$ plane, the position error in the x-direction is about ± 0.0006, actually about ± 600 km. The position errors between the perturbed and unperturbed DRO orbits in the x direction at different times are plotted, as shown in Figure 20. It shows that although the perturbed DRO orbit is stable around the original DRO orbit, the orbit position error shows an increasing trend. Therefore, it is still necessary to maintain the orbit in a timely manner.

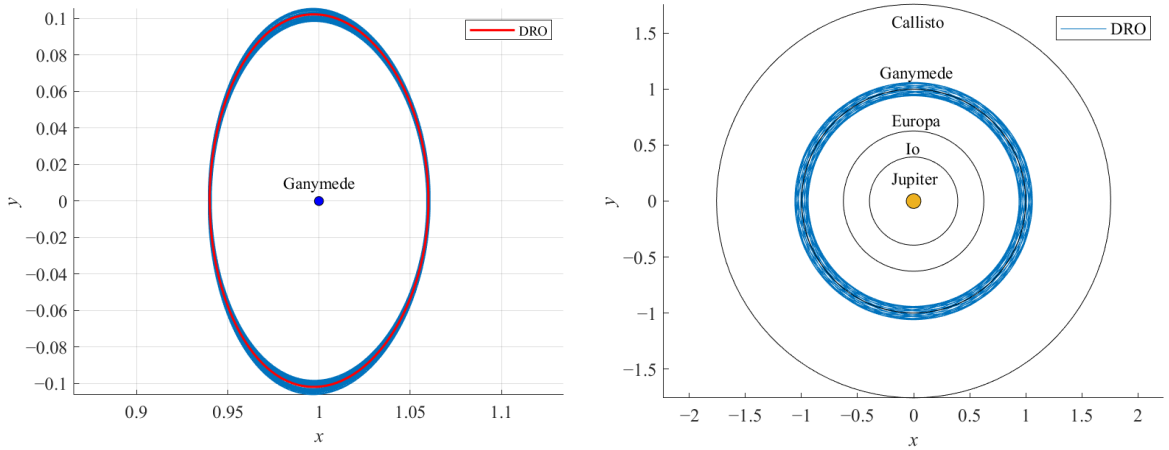

Figure 19. Perturbed DRO ($\boldsymbol{X}_0 = [0.9400, 0, 0, 0, 0.13208, 0]^{\mathrm{T}}$, $J = 2.996155$) with $\theta_{i0} = 0$ and $\theta_{s0} = 0$: (**a**) in the Jupiter–Ganymede rotating frame and (**b**) in the inertial frame.

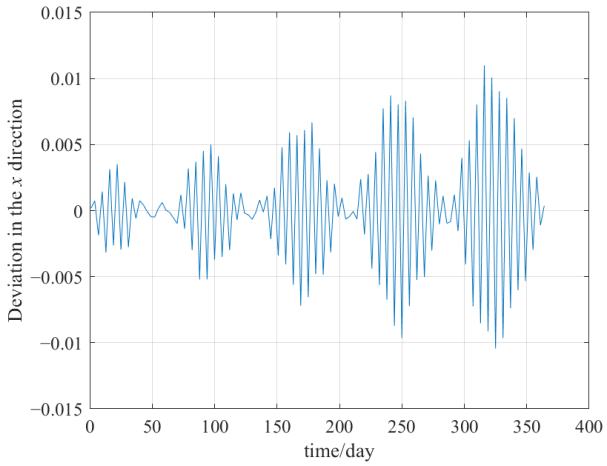

Figure 20. The deviation in the x direction over time (days) between the perturbed and unperturbed DRO ($\boldsymbol{X}_0 = [0.9400, 0, 0, 0, 0.13208, 0]^{\mathrm{T}}$, $J = 2.996155$).

Furthermore, we consider the motions of period-tripling DRO bifurcating orbits under the gravitational perturbations and find that for some of these orbits, they will quickly move away from the original orbit and diverge outward after being affected by the perturbations (Figure 21a), while some can maintain their orbit for a long period of time without diverging within a certain range, and become quasi-periodic orbits (Figure 21b). This behavior is related to the stability of the orbits, which will be explained briefly in the next subsection.

In addition, this is also related to the structure of the orbit. When the altitude relative to Ganymede is higher, the perturbation effect is stronger.

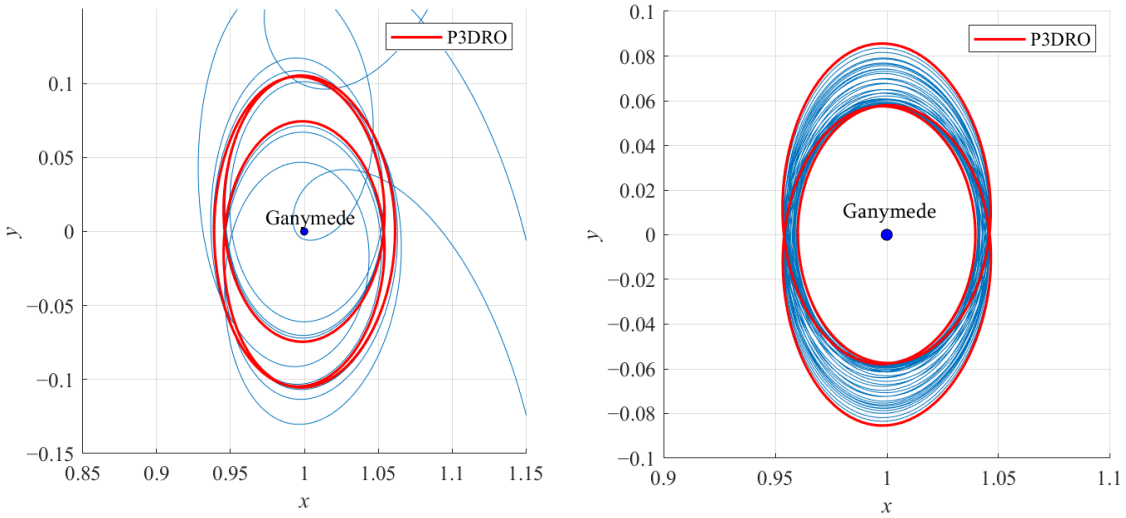

(**a**) (**b**)

Figure 21. Perturbed P3DRO with $\theta_{i0} = 0$ and $\theta_{s0} = 0$: (**a**) $\boldsymbol{X}_0 = [0.939,0,0,0,0.13190256,0]^{\mathrm{T}}$, $J = 2.996546$ and (**b**) $\boldsymbol{X}_0 = [0.96,0,0,0,0.103373313,0]^{\mathrm{T}}$, $J = 2.997904$.

3.4. Manifold Structures

Often leveraged to generate the initial guesses for transfer orbit design in the CR3BP, manifolds offer pathways for approaching and departure from unstable periodic orbits. The stability of period-multiplying bifurcating orbits has been analyzed in the previous subsection. It was found that the P3DRO family possesses the largest range for the maximum stability index. Thus, taking the period-tripling bifurcation as an example, we select different orbits with the maximum stability indices of $\nu_{\max} = 26.2387$, 10.1016, and 3.0858, and choose several initial points uniformly distributed on these orbits, then plot their stable manifold structures ($\varepsilon = 10^{-4}$, about 100 km) with two periodic lengths under the CR3BP model, as shown in Figure 22.

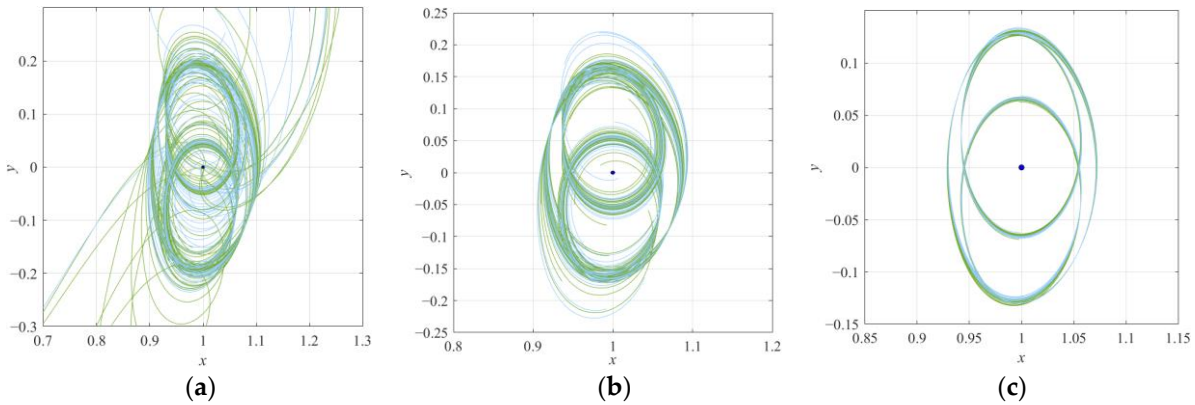

(**a**) (**b**) (**c**)

Figure 22. Stable manifold structures of P3DRO in two periods: (**a**) $\boldsymbol{X}_0 = [0.9025, 0, 0, 0, 0.19642833, 0]^{\mathrm{T}}$, $\nu_{\max} = 26.2387$, (**b**) $\boldsymbol{X}_0 = [0.9155, 0, 0, 0, 0.17223724, 0]^{\mathrm{T}}$, $\nu_{\max} = 10.1016$, and (**c**) $\boldsymbol{X}_0 = [0.9295, 0, 0, 0, 0.14750765, 0]^{\mathrm{T}}$, $\nu_{\max} = 3.0858$.

This shows that the magnitude of the stability index is directly related to the rate of the departing/approaching flows. Those orbits that possess small stability indices (generally $\nu_{\max} < 5$) depart from/approach their original orbits very slowly when affected

by small disturbances, which can be considered approximately linearly stable. The larger the maximum stability index, the more significant the manifold structure and the faster it deviates from the original orbit.

Furthermore, we investigated the manifold structures of engineering significance, the methodology for which is mentioned in Section 2.5. We selected a part of stable manifolds near the period-tripling bifurcation orbit ($\boldsymbol{X}_0$ = [0.9025, 0, 0, 0, 0.19642833, 0]$^{\mathrm{T}}$, J = 2.993305); the integration duration is three times that of the original orbital periods. We selected some points on the original orbit for integration, terminating when the orbits crossed the plane x = 0, and drew their stable manifolds. The initial point of integration is selected as the point on the orbit when the initial value of the original orbit runs for 1.4~1.7 days; their stable manifold structures are shown in Figure 23a. The initial point of integration was selected as the point on the orbit when the initial value of the original orbit runs for 11.0~11.4 days; their stable manifold structures are shown in Figure 23b. The manifolds of these parts of the orbit will come close to the orbit of Europa or Callisto after 20~30 days, so there is the possibility of a fast low-energy transfer between the Galilean moons.

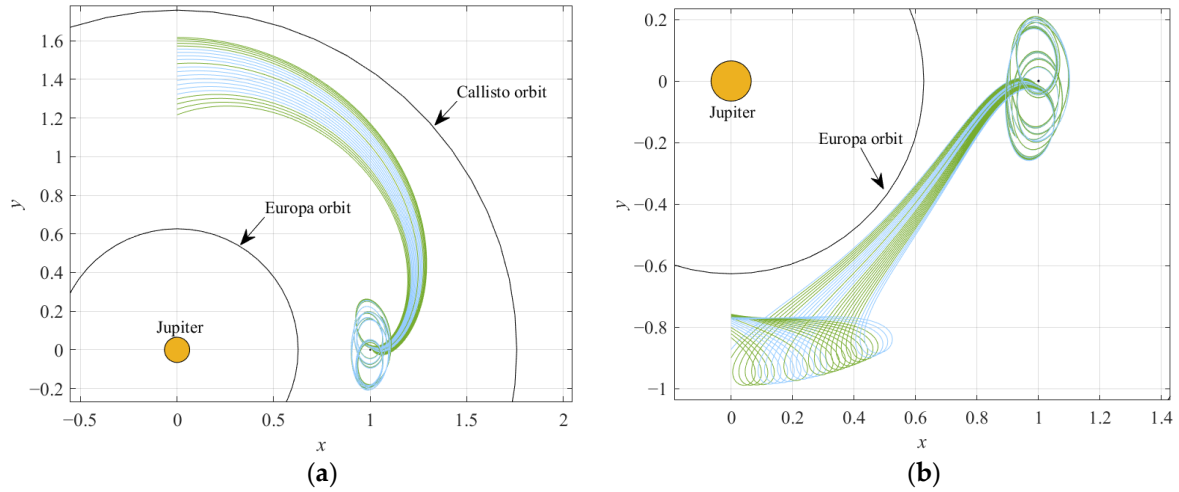

Figure 23. Partial stable manifold of P3DRO ($\boldsymbol{X}_0$ = [0.9025, 0, 0, 0, 0.19642833, 0]$^{\mathrm{T}}$, J = 2.993305): (**a**) stable manifolds within 1.4~1.7 days and (**b**) stable manifolds within 11.0~11.4 days.

Since the manifold structures of the period-multiplying bifurcation orbits are relatively complex, we use a Poincaré section to draw the coordinates of the stable manifold crossing the plane y = 0, as shown in Figure 24, with coordinates x and v_x. The red points in this figure represent the periodic orbit itself. With this information, suitable points can be selected as the starting point, according to the engineering requirement for transfer orbit design.

Figure 25 shows the difference in velocity between the period-multiplying bifurcating orbits and DROs sharing the same initial positions. Figure 26 shows the average period of the period-multiplying bifurcating orbits and the period of DROs. Existing studies usually considered using the horizontal Lyapunov orbits (HLOs) near L_1 or L_2 to transfer to DROs. From this, we can see that the difference between the initial velocities of the DRO and period-tripling bifurcating orbit is smaller than that between the DRO and Lyapunov orbit. This means that the velocity increment required to enter or leave the DRO via the period-multiplying bifurcating orbits is smaller, and the probe can still have greater energy. At the same time, although the average period of the period-multiplying bifurcating orbits is shorter in most cases, their orbital periods increase almost in multiples; thus, the overall transfer time may be longer. Therefore, trade-offs should be made based on the requirements of the practical mission.

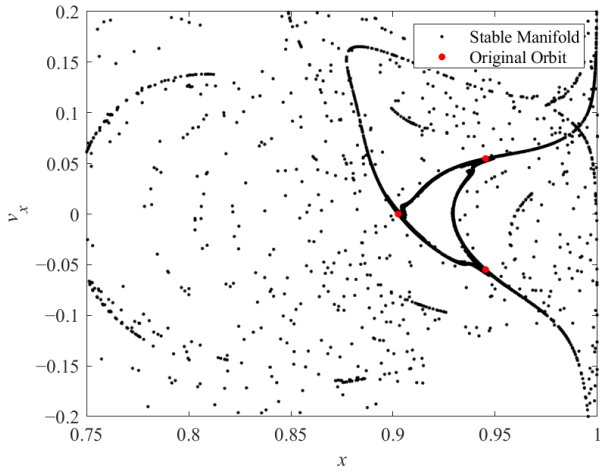

Figure 24. Stable manifold of P3DRO ($\boldsymbol{X}_0$ = [0.9025, 0, 0, 0, 0.19642833, 0]$^{\mathrm{T}}$, J = 2.993305), mapped on a Poincaré section where y = 0 in eight periods.

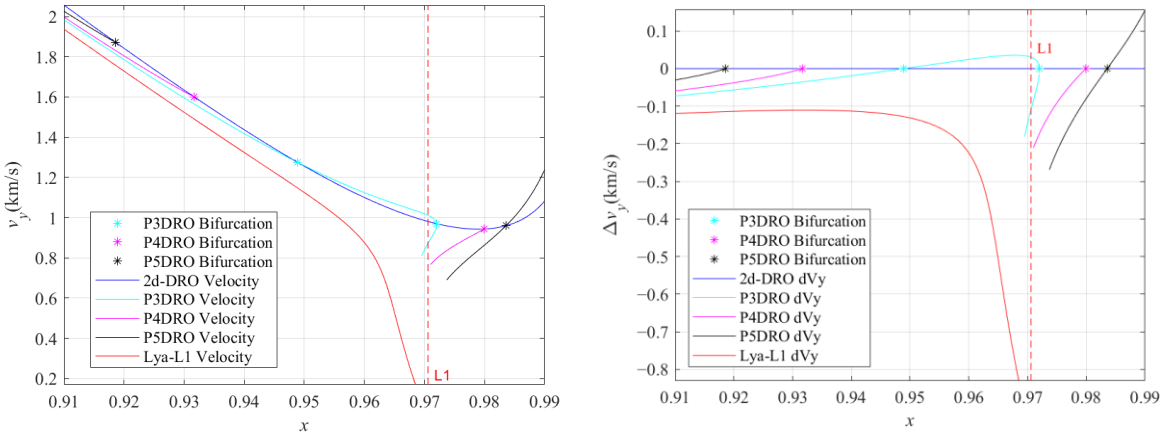

(**a**) (**b**)

Figure 25. (**a**) Relationship between the initial position and initial velocity of different orbital types and (**b**) the difference in initial velocity between the DROs and the different orbital types.

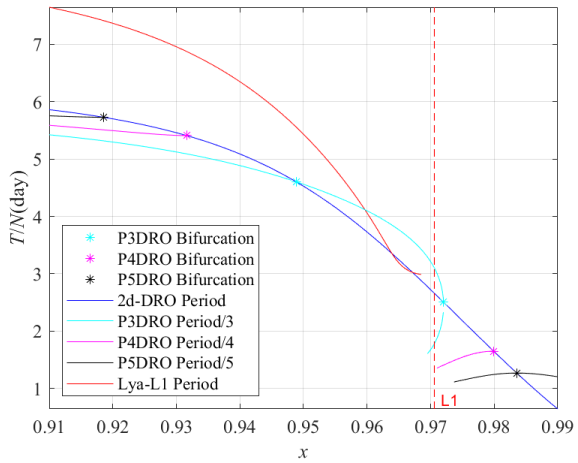

Figure 26. The average period of different orbital types.

As mentioned above, a portion of the P3DRO family shows obvious instability, and the manifolds near the orbit can be used to design the trajectory entering or leaving the DRO.

Note that the period-tripling bifurcation terminates near L_1; hence, the manifolds of period-quadrupling and period-quintupling bifurcation or other transfer methods should be considered when a lower-altitude orbit from Ganymede is needed. In addition, considering the difference in energy levels between the different Galilean moons, the manifold structures of the period-multiplying bifurcating orbits can be spliced with the manifold structures of Lyapunov orbits to design low-energy transfers.

4. Conclusions

This paper focuses on investigating the characteristics of DROs and higher-period orbits in the Jupiter–Ganymede system. Bifurcation theory was chosen to detect new families of higher-period orbits near to the DROs. Orbital stability and the invariant manifolds of DROs and higher-period orbits were investigated, based on stability indices and manifold theory, respectively. Then, we further investigated the possibility of approaching/departing from the DROs by means of stable/unstable manifolds in the period-multiplying bifurcating orbits. We found that the DRO family is strongly stable in the Jupiter–Ganymede CR3BP, which is verified through a perturbation model, taking the gravitational perturbations of the other three Galilean moons and the Sun into account. This result indicates that the DROs in the Jupiter–Ganymede system can move nearer the desired orbit for a long time, with negligible fuel consumption for regular orbital corrections, yielding potential applications in orbiting and exploring the Galilean moons. For example, the DROs could be used to place a long-term probe to observe the activity of celestial bodies in the Jupiter system and to build and refine the ephemeris model of the Jupiter system. In addition, among the period-multiplying bifurcating orbits studied in this work, the period-tripling bifurcation was found to have the widest distribution and strongest instability. Therefore, low-energy transfers for DROs can be designed by using the invariant manifold structures near the period-tripling bifurcation. Our preliminary results show that orbital transfer using the period-multiplying bifurcating orbits requires a velocity increment that is less than when using the horizontal Lyapunov orbits, but correspondingly, the transfer time may be longer. Based on this characteristic, some low-energy transfers can be designed by splicing the manifolds of the period-multiplying bifurcating orbits and the horizontal Lyapunov orbits. The discovery of unstable period-multiplying orbits around the DROs also implies the feasibility of a low-energy manifold-to-manifold trajectory that passes by the major moons of Jupiter. For these possibilities, orbiting and exploring missions from DROs around the Galilean moons can be further designed, and low-energy transfer in the vicinity of DROs in a higher-fidelity ephemeris model can be further investigated.

Author Contributions: Q.L. completed the computation of orbits and the analysis of orbital stability, conceived the paper, and wrote most of it; Y.T. completed the computation of orbits and the verification in a perturbation model, analyzed the application of manifold structures, and wrote a small part of the paper; F.J. supervised the overall work, and reviewed and modified the paper. The academic contributions of Q.L. and Y.T. are equally important. All authors have read and agreed to the published version of the manuscript.

Funding: This work was supported by the National Natural Science Foundation of China (Grants. U21B2050 and 12022214) and the Student Research Training project of Tsinghua University.

Institutional Review Board Statement: Not applicable.

Informed Consent Statement: Not applicable.

Data Availability Statement: The data presented in this study are available on request from the corresponding author.

Conflicts of Interest: The authors declare no conflict of interest.

References

1. Hénon, M. Numerical Exploration of the Restricted Problem 5, Hill's Case: Periodic Orbits and Their Stability. *Astron. Astrophys.* **1969**, *1*, 223–238.
2. Brophy, J.R.; Friedman, L.; Culick, F. Asteroid Retrieval Feasibility. In Proceedings of the 2012 IEEE Aerospace Conference, Big Sky, MT, USA, 3–10 March 2012; pp. 1–16.
3. McGuire, M.L.; Strange, N.J.; Burke, L.M.; McCarty, S.L.; Lantoine, G.B.; Qu, M.; Shen, H.; Smith, D.A.; Vavrina, M.A. Overview of the Mission Design Reference Trajectory for NASA's Asteroid Redirect Robotic Mission. In Proceedings of the AAS/AIAA Astrodynamics Specialist Conference, Stevenson, WA, USA, 23 October 2017.
4. Howell, S.M.; Pappalardo, R.T. NASA's Europa Clipper-a mission to a potentially habitable ocean world. *Nat. Commun.* **2020**, *11*, 1–4. [CrossRef] [PubMed]
5. Grasset, O.; Dougherty, M.K.; Coustenis, A.; Bunce, E.J.; Erd, C.; Titov, D.; Blanc, M.; Coates, A.; Drossart, P.; Fletcher, L.N.; et al. jUpiter iCy moons Explorer (JUICE): An ESA mission to orbit Ganymede and to characterize the Jupiter system. *Planet. Space Sci.* **2013**, *78*, 1–21. [CrossRef]
6. Kawakatsu, Y.; Kuramoto, K.; Ogawa, N.; Ikeda, H.; Mimasu, Y.; Ono, G.; Sawada, H.; Yoshikawa, K.; Imada, T.; Otake, H.; et al. Mission concept of Martian Moons eXploration (MMX). In Proceedings of the 68th International Astronautical Congress, Adelaide, Australia, 25–29 September 2017.
7. Baresi, N.; Dell'Elce, L.; Cardoso dos Santos, J.; Yasuhiro, K. Orbit Maintenance of Quasi-Satellite Trajectories via Mean Relative Orbit Elements. In Proceedings of the 69th International Astronautical Congress, Bremen, Germany, 1–5 October 2018.
8. Hénon, M. Numerical exploration of the restricted problem. vi. hill's case: Non-periodic orbits. *Astron. Astrophys.* **1970**, *9*, 24–36.
9. Broucke, R. *Periodic Orbits in the Restricted Three-Body Problem with Earth-Moon Masses*; NASA-JPL Technical Report; California Institute of Technology: Pasadena, CA, USA, 15 February 1968.
10. Benest, D. Effects of the mass ratio on the existence of retrograde satellites in the circular plane restricted problem. *Astron. Astrophys.* **1974**, *32*, 39–46.
11. Benest, D. Effects of the mass ratio on the existence of retrograde satellites in the circular plane restricted problem. II. *Astron. Astrophys.* **1975**, *45*, 353–363.
12. Benest, D. Effects of the mass ratio on the existence of retrograde satellites in the circular plane restricted problem. III. *Astron. Astrophys.* **1976**, *53*, 231–236.
13. Hénon, M. Vertical Stability of Periodic Orbits in the Restricted Problem. I. Equal Masses. *Astron. Astrophys.* **1973**, *28*, 415–426.
14. Hénon, M. Vertical Stability of Periodic Orbits in the Restricted Problem. II. Hill's Case. *Astron. Astrophys.* **1974**, *30*, 317–321.
15. Bezrouk, C.J.; Parker, J. Long Duration Stability of Distant Retrograde Orbits. In Proceedings of the AIAA/AAS Astrodynamics Specialist Conference, San Diego, CA, USA, 4–7 August 2014.
16. Bezrouk, C.J.; Parker, J. Long term evolution of distant retrograde orbits in the Earth-Moon system. *Astrophys. Space Sci.* **2017**, *362*, 176–186. [CrossRef]
17. Lara, M. Nonlinear librations of distant retrograde orbits: A perturbative approach—The Hill problem case. *Nonlinear Dyn.* **2018**, *93*, 2019–2038. [CrossRef]
18. Welch, C.M.; Parker, J.S.; Buxton, C. Mission considerations for direct transfers to a distant retrograde orbit. *J. Astronaut. Sci.* **2015**, *62*, 101–124. [CrossRef]
19. Demeyer, J.; Gurfil, P. Transfer to Distant Retrograde Orbits Using Manifold Theory. *J. Guid. Control. Dyn.* **2007**, *30*, 1261–1267. [CrossRef]
20. Perozzi, E.; Ceccaroni, M.; Valsecchi, G.B.; Rossi, A. Distant retrograde orbits and the asteroid hazard. *Eur. Phys. J. Plus* **2017**, *132*, 367–375. [CrossRef]
21. Tan, M.; Zhang, K.; Wang, J. Strategies to capture asteroids to distant retrograde orbits in the Sun–Earth system. *Acta Astronaut.* **2021**, *189*, 181–195. [CrossRef]
22. Lam, T.; Hirani, A.N.; Kangas, J.A. Characteristics of transfers to and captures at Europa. In Proceedings of the 16th AAS/AIAA Space Flight Mechanics Meeting, Tampa, FL, USA, 1 December 2006.
23. Lam, T.; Whiffen, G.J. Exploration of distant retrograde orbits around Europa. *Am. Astronaut. Soc. Pap.* **2005**, *120*, 135–153.
24. McCarthy, B.P.; Howell, K.C. Leveraging quasi-periodic orbits for trajectory design in cislunar space. *Astrodynamics* **2021**, *5*, 139–165. [CrossRef]
25. Howell, K.C. Three-Dimensional, Periodic, 'Halo' Orbits. *Celest. Mech.* **1984**, *32*, 53–71. [CrossRef]
26. Roy, A.E.; Ovenden, M.W. On the Occurrence of Commensurable Mean Motions in the Solar System: The Mirror Theorem. *Mon. Not. R. Astron. Soc.* **1955**, *115*, 296–309. [CrossRef]
27. Robin, I.A.; Markellos, V.V. Numerical determination of three-dimensional periodic orbits generated from vertical self-resonant satellite orbits. *Celest. Mech.* **1980**, *21*, 395–434. [CrossRef]
28. Markellos, V.V. Bifurcations of planar to three-dimensional periodic orbits in the general three-body problem. *Celest. Mech.* **1981**, *25*, 3–31. [CrossRef]
29. Papadakis, K.E.; Markellos, V.V. On basic families of three-dimensional periodic orbits of three massive bodies and their stability. *Astrophys. Space Sci.* **1992**, *191*, 223–229. [CrossRef]
30. Russell, E.J. Global Search for Planar and Three-Dimensional Periodic Orbits near Europa. *J. Astronaut. Sci.* **2006**, *54*, 199–226. [CrossRef]

31. Zimovan, E.M. Characteristics and Design Strategies for Near Rectilinear Halo Orbits Within the Earth-Moon System. Master's Thesis, Purdue University, West Lafayette, IN, USA, August 2017; p. 171.
32. Howell, K.; Campbell, E. Three-dimensional periodic solutions that bifurcate from halo families in the circular restricted three-body problem. *Am. Astronaut. Soc. Pap.* **1999**, *102*, 891–910.
33. Zimovan-Spreen, E.M.; Howell, K.C.; Davis, D.C. Near rectilinear halo orbits and nearby higher-period dynamical structures: Orbital stability and resonance properties. *Celest. Mech. Dyn. Astron.* **2020**, *132*, 28–53. [CrossRef]
34. Thomas, C.E.; Howell, K.C. Bifurcations from Families of Periodic Solutions in the Circular Restricted Problem with Application to Trajectory Design. Master's Thesis, Purdue University, West Lafayette, IN, USA, 1999; p. 186.
35. Broucke, R. Stability of periodic orbits in the elliptic, restricted three-body problem. *AIAA J.* **1969**, *7*, 1003–1009. [CrossRef]
36. Capdevila, L.R.; Howell, K.C. A transfer network linking Earth, Moon, and the triangular libration point regions in the Earth-Moon system. *Adv. Space Res.* **2018**, *62*, 1826–1852. [CrossRef]
37. Natasha, B.; Howell, K.C. Leveraging Natural Dynamical Structures to Explore Multi-Body Systems. Master's Thesis, Purdue University, West Lafayette, IN, USA, 2016; p. 252.
38. Cardoso dos Santos, J.; Carvalho, J.P.S.; Prado, A.F.B.A.; De Moraes, R.V. Searching for less perturbed elliptical orbits around Europa. *J. Phys. Conf. Ser.* **2015**, *641*, 012011. [CrossRef]